Nuclear Inst. and Methods in Physics Research, A 990 (2021) 164989

Contents lists available at ScienceDirect

Nuclear Inst. and Methods in Physics Research, A

journal homepage: www.elsevier.com/locate/nima

Determination of the neutron yield of Be, V and Ta targets irradiated with protons (22-42 MeV) by means of prompt gamma neutron activation analysis

Marius Rimmler [a,b,*], Johannes Baggemann [c], Sarah Böhm [d], Paul-Emmanuel Doege [c], Olaf Felden [b], Nils-Oliver Fröhlich [b], Ralf Gebel [b], Jiatong Li [c], Jingjing Li [c], Eric Mauerhofer [c], Ulrich Rücker [c], Mathias Strothmann [c], Yury Valdau [b], Paul Zakalek [c], Thomas Gutberlet [c], Thomas Brückel [a,c]

[a] Lehrstuhl für Experimentalphysik IV C, RWTH Aachen, 52062 Aachen, Germany
[b] Institut für Kernphysik (IKP-4), Forschungszentrum Jülich GmbH, 52425 Jülich, Germany
[c] Jülich Centre for Neutron Science (JCNS-2), Forschungszentrum Jülich GmbH, 52425 Jülich, Germany
[d] NET, RWTH Aachen, 52062 Aachen, Germany

ARTICLE INFO

Keywords:
Neutron yield
PGNAA
Be, V and Ta target

ABSTRACT

The neutron yield for beryllium, vanadium and tantalum irradiated with 22, 27, 33 and 42 MeV protons is indirectly determined by Prompt Gamma Neutron Activation Analysis (PGNAA). The neutron-to-gamma conversion rate is measured with an AmBe calibration neutron source. Corrections by escaped neutrons are applied via MCNP simulations of the experiment using the ENDF/B-VII.1 database. The experimental results are in good agreement with the neutron yield obtained from simulations deviating by 0.4% to 13%.

1. Introduction

Within the last decades, neutron scattering and neutron analytics have proven to be powerful tools for the observation of complex phenomena in condensed and soft matter science with impacts on innovations in our everyday life [1]. High power Compact Accelerator-driven Neutron Sources (CANS) represent a promising new type of neutron source to fill the gap in neutron provision by the ongoing demise of older research reactors and to support the efficient use of future flagship facilities as the European Spallation Source (ESS) [2]. In CANS, a primary proton beam in the sub-100-MeV energy range impinges on a metal target generating neutrons via nuclear reactions. At Forschungszentrum Jülich GmbH, the High-Brilliance neutron Source project (HBS) aims to develop a pulsed medium-flux, high brilliance accelerator-driven neutron source facility based on a high current linear proton accelerator, scalable up to 70 MeV proton energy and optimized to deliver high brilliance neutron beams to a large variety of neutron instruments [3,4]. For HBS, the target material should provide the largest neutron yield and thus highest brilliance, both depending on the energy of the sub-100 MeV primary proton beam. Calculations using the TALYS nuclear code [5] suggest that low-Z materials, e.g. Be and V, generate more neutrons at proton beam energies below 20 MeV while high-Z materials, e.g. Ta, generate more neutrons at proton beam energies above [6], when considering the (p,n) reaction channel with a target thickness adapted to the proton-energy-dependent penetration depth. However, previous experiments on the neutron yield of Be irradiated by protons with energies ranging from 14.8 MeV to 80 MeV based on time-of-flight techniques [7,8] as well as on the "manganese bath" technique [9,10] show differing results when compared with each other as well as with the calculations from [6].

In this work, we present the experimental determination of the total neutron yield, i.e. taking into account all the reaction channels that generate neutrons, for 22, 27, 33, 42 MeV protons on Be, V and Ta targets. We have introduced a novel method (Section 3) for the experimental determination of the neutron yield via measurement of the 2.2 MeV prompt gamma-ray of hydrogen induced by thermal neutron capture in a polyethylene moderator. Simulations of the experiment with MNCP [11] and the ENDF/B-VII.1 database [12] are performed in order to apply corrections to the measurements and to access the proton induced neutron yield, i.e. considering only neutrons from the (p,n) reaction channel. Finally, we compare the simulated total and proton induced neutron yield with the experimental results in order to improve the reliability of the underlying databases for the target material selection in future CANS projects.

2. Experimental setup

The experimental setup for the determination of the neutron yield has been installed at the COSY (COoler SYnchrotron) accelerator facility at Forschungszentrum Jülich GmbH [13]. The proton beam at

* Corresponding author at: Lehrstuhl für Experimentalphysik IV C, RWTH Aachen, 52062 Aachen, Germany.
E-mail address: m.rimmler@fz-juelich.de (M. Rimmler).

https://doi.org/10.1016/j.nima.2020.164989
Received 19 November 2020; Received in revised form 16 December 2020; Accepted 23 December 2020
Available online 28 December 2020

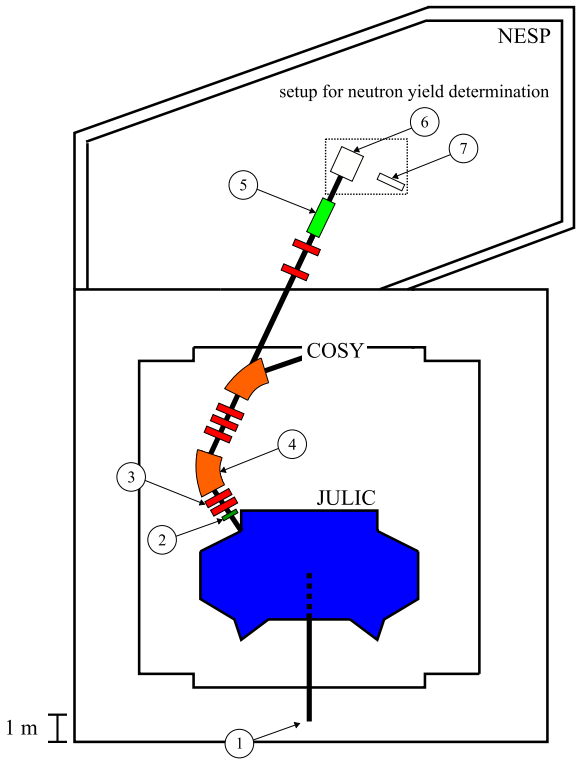

Fig. 1. Layout of the COSY injector JULIC with associated low energy irradiation site NESP including a schematic of the experimental setup used for neutron yield determination (6 + 7). 1: multi cusp filament volume source, 2: moveable graphite degrader, 3: quadrupole magnet, 4: dipole magnet, 5: non-destructive diagnostics, i.e. beam position monitor (BPM) and fast current transformer (FCT), 6: polyethylene moderator cylinder including target holder and target current measurement and 7: gamma spectroscopy system.

energies ranging from 22 MeV to 42 MeV, which was utilized during the neutron yield determination experiments, is supplied by the injector cyclotron JULIC (JUelich Light Ion Cyclotron) of the synchrotron COSY. The isochronous sector magnet cyclotron JULIC routinely provides unpolarized and polarized H^- and D^- at 45 MeV and 76 MeV, respectively, with a maximum beam current of 10 μA [14,15]. For the experiment discussed in this work, unpolarized H^- is supplied by a multi cusp filament volume source. A source beam line connects the ion source to the cyclotron as shown in Fig. 1. Setting JULIC to 45 MeV H^- in combination with a tuneable graphite degrader delivers 22, 27, 33 and 42 MeV protons for the experiment. The corresponding energies were measured to be correct within 1 MeV energy uncertainty by determining the propagation depth of the proton beam in a PMMA cube via a GAFchromic film [16] (see supplementary material Section S2).

The proton beam is sent to the experimental area at the low energy irradiation site (NiederEnergiebeStrahlungsPlatz - NESP) with a set of quadrupoles and one 38.25° sector bending dipole magnet while traversing a second identical dipole magnet without deflection, which is used when injecting into COSY as shown in Fig. 1. In the NESP area, a set of non-destructive beam diagnostics, including a beam position monitor (BPM) and a fast current transformer (FCT) is installed [17]. The beamline is connected to the experimental setup for neutron yield determination containing primarily a polyethylene moderator cylinder, including the targets and a Faraday cup type current measurement, as well as a gamma spectroscopy system. The horizontally and vertically projected proton beam profile is approximated gaussian with full width at half maximum (FWHM) ranging from 20 mm to 43 mm for 42 MeV to 22 MeV, respectively, measured with a multi wire proportional chamber (MWPC, see supplementary material Section S1).

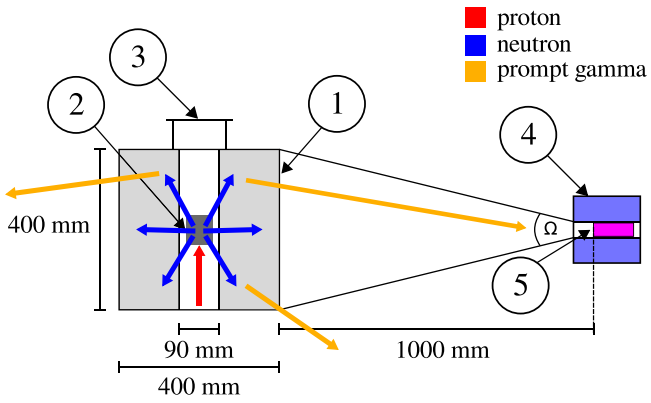

Fig. 2. Sketch of the experimental setup, as positioned in Fig. 1, for the determination of the neutron yield via prompt gamma spectroscopy. 1: polyethylene moderator cylinder with 400 mm length, 400 mm outer diameter and 90 mm inner diameter, 2: target holder with targets as listed in Table 2 with electronic connection to a picoammeter, 3: Kapton vacuum window , 4: lead collimator cylinder with copper inner layer, 5: HPGe-detector. The HPGe-detector and the lead collimator are positioned such that a solid angle Ω includes the whole polyethylene moderator cylinder.

The experimental setup for neutron yield determination is shown schematically in Fig. 2. The protons impinge on exchangeable Be, V or Ta targets. The Be target is a massive cylinder with a radius of 35 mm and a thickness of 100 mm. The V and Ta targets are disks with a radius of 40 mm and thicknesses ranging between 2.56 mm to 4.54 mm for V and between 1.6 mm to 3 mm for Ta in order to account for the increasing penetration depth of protons with an energy of 22 MeV to 42 MeV, respectively. The targets are positioned individually in the middle of a 400 mm long hollow polyethylene cylinder with a wall thickness of 155 mm acting as fast neutron moderator. The proton beam current on the target is monitored with a calibrated current amplifier (Keithley 18000-20). Just before the target, the proton beam passes a set of non-destructive diagnostics, which allows to perform beam current measurements without a target. This gives the possibility to extrapolate the proton beam current that would have been measured on a target during the background measurements where no target is installed. The targets are placed inside vacuum with a thin Kapton foil exit window behind the polyethylene moderator which allows to perform background measurements with minimal influence from the passing proton beam.

The total neutron yield is determined via gamma-ray spectrometry measuring the count rate of the 2.2 MeV prompt gamma line of hydrogen induced by thermal neutron capture in the polyethylene moderator. The gamma-ray spectrometer consists of a high purity germanium (HPGe) coaxial detector (Canberra GR1020 with relative efficiency of 10%, energy resolution of 2.2 keV at 1.32 MeV for 6 μs shaping time) shielded with a cylindrical lead collimator with an opening diameter of 125 mm and a wall thickness of 80 mm. The gamma-ray spectrometer is positioned perpendicularly to the proton beam axis at mid-height of the target. The distance between the collimated HPGe-detector and the outer surface of the polyethylene moderator is 1 m ensuring that the whole volume of the moderator is seen by the detector. The signals of the detector preamplifier are processed through a digital spectrometer (XiA Polaris). The gamma-ray spectra are recorded for 1 to 2 h (real time) and analysed with Gamma-W software [18]. The proton beam intensity is adjusted such that the live time of the detector is around 80% or larger of the real time of the measurement. As an example the prompt gamma-ray spectra recorded during irradiation with 42 MeV protons with and without Be target are shown in Fig. 3. The identified isotopes are given on the spectra. The spectrum recorded with the Be target is dominated by the prompt gamma line of hydrogen (H-1) (Fig. 3c). The prompt gamma lines of carbon (C-12) induced by thermal neutron capture and by inelastic scattering of fast neutrons in

the polyethylene moderator are also observed (Fig. 3d). The remaining gamma lines are induced by interaction of slow and fast neutrons escaping the moderator with the HPGe-detector (Ge, In), the collimator shielding (Pb, Cu) and surrounding structural materials (Al, Fe, Cr). The same gamma lines with lower count rates are also observed in the spectrum recorded without the Be target. The spectra recorded for all targets at various proton energies show the same gamma-ray signature with the exception of some target-specific characteristics such as gamma lines for inelastic neutron scattering of fast neutrons from V in the case of the V target which do not influence the determination of the neutron yield.

3. Method

The target total neutron yield Y (s^{-1} mA^{-1}) is determined from the measured count rate of the 2.2 MeV prompt gamma line of hydrogen induced by thermal neutron capture in the polyethylene moderator and using an AmBe source of well-known neutron emission for calibration as follows:

$$Y = \left[\frac{Z_{\text{target}}}{I_{\text{target}}} - \frac{Z_{\text{no target}}}{I_{\text{no target}}}\right] \cdot \frac{N_{\text{AmBe}}}{Z_{\text{AmBe}}} \cdot \frac{f_{\text{AmBe}}}{f_{\text{target}}} \cdot \frac{g_{\text{AmBe}}}{g_{\text{target}}} \tag{1}$$

with Z (s^{-1}) being the count rate of the 2.2 MeV gamma line, I (mA) the average proton beam current measured on the target or extrapolated from the non-destructive current measurement in the case of the measurements without target and $N_{\text{AmBe}} = 2.59 \times 10^4\ s^{-1}$ being the neutron emission of the AmBe source (Amersham Buchler, $N_{\text{AmBe}} = 2.8 \times 10^4\ s^{-1}$ at 10 mCi in 1970, $T_{1/2} = 433$ y). f is a correction factor for neutrons leaving the system and not contributing to the production of 2.2 MeV photons which is given by

$$f = 1 - n_{\text{escape}}, \tag{2}$$

where n_{escape} is the fraction of neutrons escaping the polyethylene moderator. In Eq. (1), g is a correction factor related to the geometrical efficiency for the detection of 2.2 MeV photons which is expressed by

$$g = \frac{p}{f}, \tag{3}$$

where p is the total number of 2.2 MeV photons emitted from the polyethylene moderator towards the HPGe-detector normalized to the neutrons generated from the target or AmBe source. Therefore, $p_{\text{AmBe}}/p_{\text{target}}$ represents the overall correction of the experiment in terms of efficiency when comparing the measurements with target and with AmBe calibration source in Eq. (1). Note that the correction is applied as ratio of correction factors for the target and for the AmBe measurements, such that it does not need to be considered that not all neutrons absorbed in the polyethylene moderator contribute to the production of 2.2 MeV photons.

The measured values of the count rate Z and of the current I, are given in Table 2. The values of n_{escape} and p are estimated numerically in the simulation part below.

4. Simulation of neutron yield measurement

4.1. Simulation setup

The simulation of the experiment as described in Section 2 is carried out with the Monte-Carlo N-Particle Transport Code (MCNP) [11]. The corresponding cross section data is based on the Evaluated Nuclear Data File database (ENDF/B-VII.1) [12]. The geometry of the simulation environment is identical to the experimental setup as shown in Fig. 2 except that the HPGe-detector is replaced by a spherical detector band with radius being the distance from the target centre to the HPGe-detector, i.e. 1200 mm, and with width being similar to the HPGe-detector entrance width, i.e. 100 mm. This allows one to speed up the computation time by taking advantage of the cylindrical symmetry of the setup. Fig. 4 shows the geometry of the simulation.

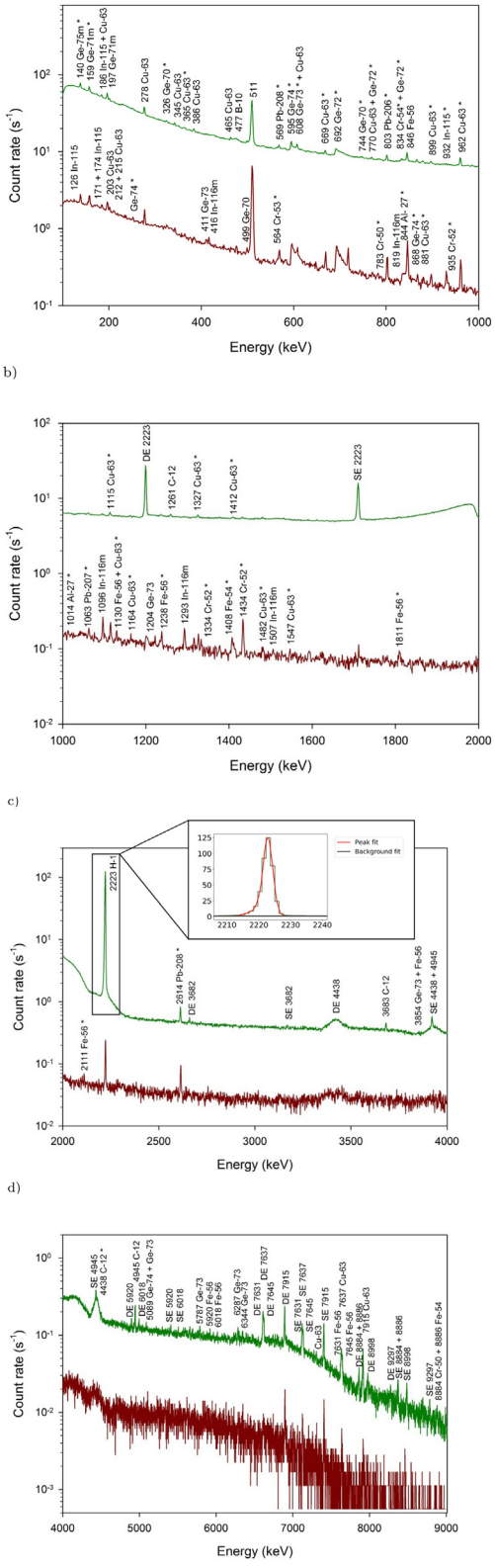

Fig. 3. Prompt gamma-ray spectra in the energy range (a) 100 – 1.000 keV, (b) 1.000–2.000 keV, (c) 2.000–4.000 keV and (d) 4.000–9.000 keV recorded with (green) and without Be target (red) for an irradiation with 42 MeV protons. The gamma lines labelled with an asterisk are induced by inelastic scattering of fast neutrons, the other being issued from neutron capture. The prompt gamma line of hydrogen (H-1) at 2.2 MeV is highlighted by the inset showing the fitted data. The live time of the measurement is 2834 s (3600 s real time) and 1780 s (1800 s real time) with and without Be target, respectively.

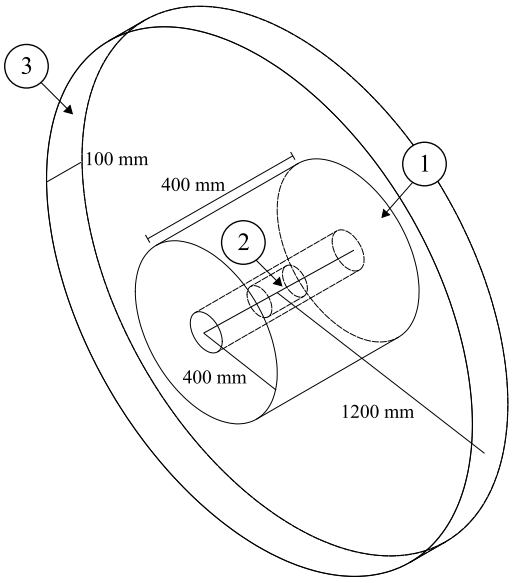

Fig. 4. Layout of the simulation geometry. 1: polyethylene moderator cylinder, 2: target, 3: gamma detector band with 1200 mm radius from the target centre and 100 mm width.

All simulations with targets are carried out with a primary proton beam with 1×10^7 protons (except for 42 MeV protons on Be, where the number of protons is limited by MCNP to 1.7×10^5 resulting into a larger statistical error) while simulations with the AmBe calibration source are performed with a virtual neutron source and 1×10^7 neutrons distributed through a neutron spectrum deduced from the specifications of the AmBe source [19]. The target thickness and diameter in the simulation geometry is adapted according to the experiment and identical to the ones in Table 2.

The relevant simulation output for the different target and energy combinations is summarized in Table 1. Here, the total neutron yield Y, the neutron yield from the (p,n)-reactions $Y_{(p,n)}$, the neutron yield from (n,2n)-reactions $Y_{(n,2n)}$ and the average neutron energy $\bar{E}_n$ are extracted from a sphere surrounding the target without polyethylene moderator in Fig. 4. n_{escape} is defined as the neutrons escaping the complete system, i.e. from a sphere surrounding target and moderator, normalized to the total number of neutrons generated from the target. The gamma correction factor g is derived from the photons at 2.2 MeV energy detected on the spherical detector band in Fig. 4.

It should be mentioned that Y represents the total neutron yield, i.e. taking into account all reaction channels that generate neutrons in the experimental setup. Y depends strongly on the geometry of the setup including the target as well as the moderator. In order to be more independent from the experimental setup, it is useful to consider additionally the proton induced neutron yield, i.e. taking into account neutrons only generated from the (p,n) reaction channel. To access the proton induced neutron yield, one has to subtract the contribution of all other reaction channels to the neutron production from the neutron yield Y. Consulting the ENDF/B-VII.1 [12] database, it turns out that the (n,2n) reaction channel is the most dominant of these reaction channels while other reaction channels are negligible. Therefore

$$Y_{(p,n)} = Y - Y_{(n,2n)} \tag{4}$$

approximates the proton induced neutron yield with $Y_{(n,2n)}$ being the neutron yield of (n,2n) reactions.

4.2. Simulation results

We focus on the results of the correction factors applied to determine the total neutron yield by means of Eq. (1). The correction factor

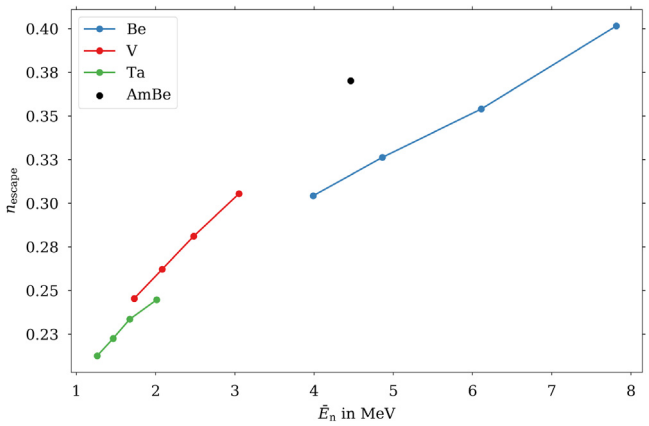

Fig. 5. Neutron escape ratio n_{escape} versus average neutron energy $\bar{E}_n$ of neutrons emerging from the targets and the AmBe calibration source. A line is drawn to guide the eye for each target material. All data taken from Table 1.

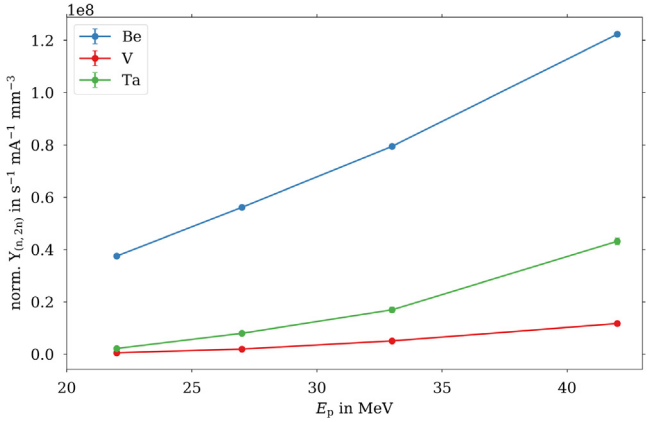

Fig. 6. Neutron yield of (n,2n) reaction channel $Y_{(n,2n)}$ normalized to the target volume versus proton energy. All data taken from Table 1.

f in Eq. (2) which takes into account the neutron escape ratio n_{escape} appears to have the greatest influence (see Table 1). We associate the neutron escape ratio with the neutron energy, assuming that neutrons emitted from the target with higher energy have a lower probability to be absorbed in the polyethylene moderator, thus escaping the moderator without generating 2.2 MeV photons. However, for all targets and for the AmBe calibration source, n_{escape} cannot solely be related to the neutron energy. The proton-energy-dependent angular distribution of the neutron emission additionally influences n_{escape} due to the geometric anisotropy of the cylindrical moderator.

From Fig. 5 showing n_{escape} versus $\bar{E}_n$, we can conclude that the neutron escape ratio nonetheless scales approximately linear with the average energy of the neutrons produced by the target. The average neutron energy itself scales with the proton energy (see Table 1) and depends on the atomic number of the target. Here, the average neutron energy is determined from the neutron spectrum of a bare target. The simulated neutron spectra of the bare targets are shown in the supplementary materials Section S3.

In summary, all simulated n_{escape}, except for Be at 42 MeV proton energy, are smaller than n_{escape} for the AmBe calibration source and therefore the correction f_{AmBe}/f_{target} primarily lowers the measured yield. Applying n_{escape} via Eq. (2) as a correction factor to the calculated total neutron yield introduces a systematic uncertainty based on the database (ENDF/B-VII.1) [12] employed in the simulations. The plausibility of the simulated n_{escape} for all targets is given by the linear

Table 1
Summary of MCNP simulation results with Y being the total neutron yield and $Y_{(p,n)}$ being the proton induced neutron yield. $Y_{(n,2n)}$ amounts for the neutron yield of (n,2n) reactions. $\bar{E}_n$ is the average neutron energy. n_{escape} represents the fraction of neutrons escaping the polyethylene moderator, p gives the total number of 2.2 MeV photons detected on the cylindrical detector band normalized to the generated neutrons and g gives a correction factor related to the detection efficiency of 2.2 MeV photons.

Target	Y (s^{-1} mA^{-1})	$Y_{(p,n)}$ (s^{-1} mA^{-1})	$Y_{(n,2n)}$ (s^{-1} mA^{-1})	$\bar{E}_n$ (MeV)	n_{escape}	p	g
22 MeV							
Be	1.251(3)E+14	1.107(3)E+14	1.44(1)E+13	4.00(6)	0.304(1)	1.38(3)E−02	1.99(4)E−02
V	0.599(2)E+14	0.599(2)E+14	7(2)E+10	1.73(4)	0.245(2)	1.50(4)E−02	1.99(5)E−02
Ta	0.494(2)E+14	0.493(2)E+14	1.8(3)E+10	1.26(3)	0.213(2)	1.49(4)E−02	1.89(6)E−02
27 MeV							
Be	1.771(3)E+14	1.555(3)E+14	2.16(1)E+13	4.86(9)	0.326(1)	1.32(2)E−02	1.96(3)E−02
V	0.914(2)E+14	0.914(2)E+14	2.5(4)E+10	2.08(6)	0.262(2)	1.45(3)E−02	1.96(4)E−02
Ta	0.931(2)E+14	0.931(2)E+14	6.4(6)E+10	1.46(5)	0.223(1)	1.50(3)E−02	1.93(4)E−02
33 MeV							
Be	2.490(4)E+14	2.184(4)E+14	3.06(1)E+13	6.1(1)	0.354(1)	1.24(2)E−02	1.91(3)E−02
V	1.400(3)E+14	1.399(3)E+14	9.4(8)E+10	2.5(1)	0.281(1)	1.44(3)E−02	2.01(4)E−02
Ta	1.669(3)E+14	1.668(3)E+14	1.7(1)E+11	1.67(9)	0.233(1)	1.44(2)E−02	1.88(3)E−02
42 MeV							
Be	3.74(4)E+14	3.27(4)E+14	4.7(1)E+13	7.8(2)	0.402(7)	1.2(2)E−02	2.0(3)E−02
V	2.328(4)E+14	2.325(4)E+14	2.7(1)E+11	3.1(2)	0.305(1)	1.36(2)E−02	1.96(3)E−02
Ta	3.143(4)E+14	3.137(4)E+14	6.5(2)E+11	2.0(1)	0.245(1)	1.44(2)E−02	1.91(2)E−02
AmBe	–	–		5(3)	0.3702(2)	1.280(4)E−02	2.030(6)E−02

behaviour between the measured photon yield of the gammas induced by interaction of slow and fast neutrons escaping the moderator with the HPGe-detector collimator with respect to the simulated yield of escaping neutrons as explained in detail in Section S4 of the supplementary material. Here, we deduce a systematic uncertainty of the simulated n_{escape} of less than 15%.

Concerning the gamma detection efficiency factor g (see Table 1) for the different energy and material combinations as well as for AmBe, we observe identical values. This suggests that the gamma-detector sees a similar gamma source and the thermal neutron cloud in the polyethylene moderator has almost similar dimensions for all experiments.

As stated in the previous subsection (see Eq. (4)), the total and proton induced neutron yield primarily differ by the contribution of the (n,2n) reaction. Looking at Table 1, it can be seen that the (n,2n) reaction yield of Be is typically between two or three orders of magnitude larger than for V and Ta. This is partly because of the large volume of the Be target with respect to the V and Ta targets, but not entirely as it can be seen when looking at the neutron yield of the (n,2n) reaction channel $Y_{(n,2n)}$ normalized to the target volume as shown in Fig. 6. Thus Be has the largest neutron yield of (n,2n) reactions for the geometry of the setup used in this work. The neutron yield of (n,2n) reactions for Be is up to 12% of the total neutron yield while it is below 0.1% of the total neutron yield for V and Ta.

5. Results

The proton-energy dependence of the experimental and simulated total and proton induced neutron yield for the different targets is shown in Fig. 7(a) and Fig. 7(b), respectively. In both cases, the simulated data agree well with the experimental ones for all targets and proton energies taking into account the uncertainties. The relative uncertainties on the measured values Y and Y(p,n) are mainly of statistical nature and vary between 6 and 18%. The results are summarized in Table 2.

The total neutron yield of Be is about a factor 2 higher than that of V over the entire range of proton energy. When compared to Ta, the gain in the total neutron emission of Be decreases with increasing proton energy from 2.6 at 22 MeV to 1.2 at 42 MeV. In the energy range 22-27 MeV, V and Ta perform similar whilst Ta exhibits a stronger increase in the total neutron yield above 30 MeV.

The proton induced neutron yield shows a similar tendency than the total neutron yield. The proton induced neutron yield of Be is higher than that of V by a factor of about 1.9 in the energy range 22–33 MeV and by a factor 1.6 at 42 MeV. When compared to Ta, the gain in the proton induced neutron emission of Be decreases with increasing proton energy from 2.2 at 22 MeV to 1.0 at 42 MeV. Thus we can expect that Ta will outperform Be at proton energies above 42 MeV.

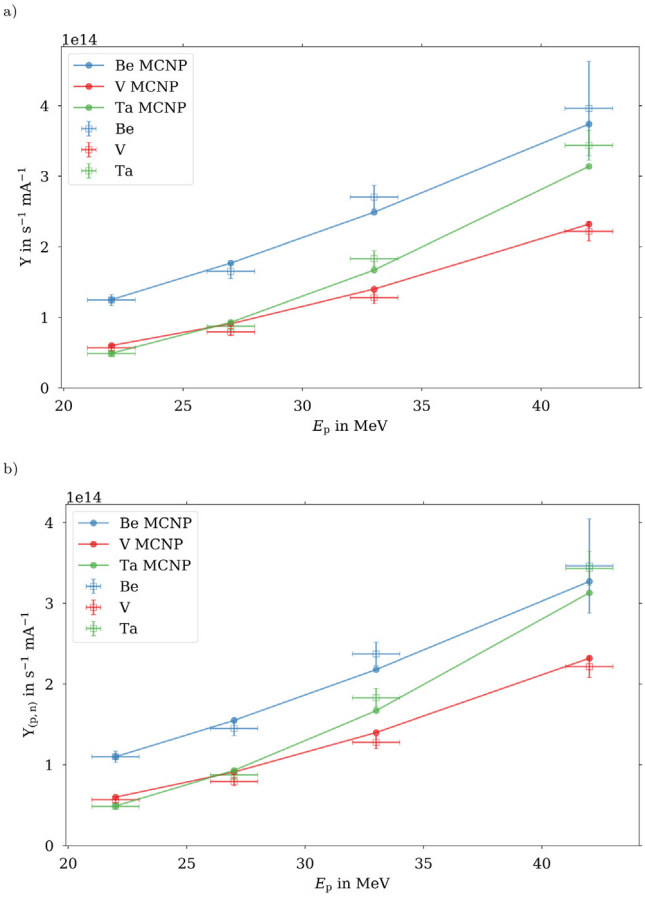

Fig. 7. (a) : Experimental total neutron yield Y (open rectangle) and simulated total neutron yield (circle). (b): Experimental proton induced neutron yield $Y_{(p,n)}$ (open rectangle) and simulated proton induced neutron yield (circle). A line for the simulation results is drawn to guide the eye. The experimental data is taken from Table 2 and the simulated data is taken from Table 1.

Table 2
Summary of experimental data, i.e. average proton beam current I and count rate for the 2.2 MeV gamma line Z, according to proton energy and target, target radius r and target length l. The neutron yield Y is calculated according to Eq. (1) and the proton induced neutron yield $Y_{(p,n)}$ according to Eq. (4).

Target	r, l (mm,mm)	I (mA)	Z (s^{-1})	Y (s^{-1} mA^{-1})	$Y_{(p,n)}$ (s^{-1} mA^{-1})
22(1) MeV					
Be	35, 100	1.474(1)E−07	22.8(3)	1.24(8)E+14	1.10(7)E+14
V	40, 2.56	1.373(1)E−07	10.6(3)	0.57(4)E+14	0.57(4)E+14
Ta	40, 1.6	1.426(1)E−07	9.4(2)	0.49(3)E+14	0.49(3)E+14
no target	–	1.4168(8)E−07	0.10(1)	–	–
27(1) MeV					
Be	35, 100	2.610(4)E−07	51.2(3)	1.7(1)E+14	1.45(9)E+14
V	40, 2.56	2.623(5)E−07	27.2(4)	0.79(5)E+14	0.79(5)E+14
Ta	40, 1.6	2.535(5)E−07	30.0(3)	0.87(6)E+14	0.87(6)E+14
no target	–	3.064(3)E−07	0.13(1)	–	–
33(1) MeV					
Be	35, 100	6.025(4)E−07	181(1)	2.7(2)E+14	2.4(1)E+14
V	40, 3.69	6.352(4)E−07	105(1)	1.28(8)E+14	1.28(8)E+14
Ta	40, 2.0	6.459(3)E−07	153(1)	1.8(1)E+14	1.8(1)E+14
no target	–	6.171(2)E−07	0.42(3)	–	–
42(1) MeV					
Be	35, 100	8.670(1)E−07	379(3)	4.0(7)E+14	3.5(6)E+14
V	40, 4.54	7.997(1)E−07	217(2)	2.2(1)E+14	2.2(1)E+14
Ta	40, 3.0	7.859(1)E−07	349(4)	3.4(2)E+14	3.4(2)E+14
no target	–	17.137(1)E−07	0.57(4)	–	–
AmBe	–	–	0.0297(18)	–	–

6. Discussion

When we compare our results for the determination of the neutron yield from a Be target irradiated with 22 MeV protons with measurements from [7] using TOF techniques ($Y = 1.50(6) \times 10^{14}\,s^{-1}mA^{-1}$), we observe that our result is a factor of 0.83(6) smaller. In [9], experiments using the "manganese bath" technique with Be and 23, 35 and 45 MeV protons result in measured total neutron yields of 1.2(1), 2.3(2) and $3.2(3) \times 10^{14}\,s^{-1}\,mA^{-1}$, respectively. We obtain results which are slightly larger but in reasonable agreement deviating by a factor of 1.0(1), 1.2(1) and 1.3(2) at the most similar measured energies of 22, 33 and 42 MeV, respectively. In the work of [10], which also uses the "manganese bath" technique, a total neutron yield of 1.77(8), 9.2(4) and $1.26(6) \times 10^{14}\,s^{-1}mA^{-1}$ for Be, V and Ta, respectively, at 32 MeV proton energy was measured. Here, at 33 MeV for the same targets, our results for Y are typically larger by a factor of 1.5(1), 1.4(1) and 1.4(1) for Be, V and Ta, respectively. A comparison of the total neutron yield for targets with a large (n,2n) contribution is generally rather difficult as it depends strongly on the experiment condition, i.e. the moderator and target geometry. The differences in the measured neutron yield, especially for Be, can most likely be attributed to this. In order to have a more consistent comparison of the values from different experiments, the proton induced neutron yield $Y_{(p,n)}$ should be considered which can unfortunately not be extracted from the literature data.

Comparing our experimental results to the analytical calculations based on the TALYS nuclear code of $Y_{(p,n)}$ in [6], the dominance of high-Z materials as Ta over low-Z materials as Be seems to be shifted from 20 MeV to higher energies (> 42 MeV) according to our work. This can be attributed to the much larger $Y_{(p,n)}$ of Be measured in our work, i.e. up to three times as large as in [6], while the measured $Y_{(p,n)}$ for V and Ta are in agreement with the analytical calculations, deviating by maximum 16 and 17%, respectively. As stated already in [6], the large deviation in $Y_{(p,n)}$ of Be can most likely be traced back to the underlying TALYS nuclear code producing inaccurate cross-sections for light elements.

An overview of literature data is given in Table S3 in the supplementary material.

7. Conclusion

A novel, fast and easy-to-handle method to determine the neutron yield of metal targets impinged by an ion beam has been introduced. The total and proton induced neutron yield of Be, V and Ta has been determined for irradiation with 22, 27, 33 and 42 MeV protons. Corrections have been applied by simulating the experiments with MCNP using the ENDF/B-VII.1 database. The measured neutron yield was compared with the neutron yield obtained from these simulations which showed good agreement.

Summarizing the experimental results, Be turns out to perform best below 42 MeV proton energy for both total and proton induced neutron yield. Especially the large (n,2n) neutron yield of Be, even when normalized to the target volume, makes it beneficial to use a thick Be target in this energy range when envisaging a maximum neutron yield. However, the results suggest a cross-over of the proton induced neutron yield from Be and Ta, where Ta seems to outperform Be at proton energies above 42 MeV. Thus, when requiring a thin target, where the contribution of (n,2n) reactions to the total neutron yield plays a minor role, Ta is more favourable in this energy range than Be. Thin targets are particularly interesting for CANS where the target thickness is often chosen such that the protons are not stopped inside the target in order to avoid target damage by blistering [20]. Be could then be used additionally around the Ta target acting as a neutron multiplicator with its strong (n,2n) neutron yield contributing to a large overall neutron yield of the combined setup.

We finally apply these findings to ongoing CANS projects. For the HBS project at Forschungszentrum Jülich GmbH, Ta is chosen as preferred material together with a 70 MeV proton beam [4]. This is supported by our experimental results for the proton induced neutron yield which suggest that Ta outperforms thin Be and V targets at proton energies above 42 MeV. The SONATE project at CEA Saclay develops a CANS with protons at 20 MeV using a thick Be target [21] which is the most efficient at this energy as affirmed by our studies.

CRediT authorship contribution statement

Marius Rimmler: Writing - original draft, Formal analysis, Data curation, Visualization, Investigation. **Johannes Baggemann:** Investigation. **Sarah Böhm:** Formal analysis. **Paul-Emmanuel Doege:** Investigation. **Olaf Felden:** Resources, Supervision. **Nils-Oliver Fröhlich:** Resources. **Ralf Gebel:** Resources, Funding acquisition. **Jiatong Li:** Formal analysis. **Jingjing Li:** Writing - review & editing, Investigation. **Eric Mauerhofer:** Writing - review & editing, Conceptualization, Investigation, Supervision. **Ulrich Rücker:** Methodology, Supervision. **Mathias**

Strothmann: Investigation. **Yury Valdau:** Resources. **Paul Zakalek:** Writing - review & editing, Data curation, Methodology, Investigation. **Thomas Gutberlet:** Writing - review & editing, Supervision. **Thomas Brückel:** Project administration, Funding acquisition.

Declaration of competing interest

The authors declare that they have no known competing financial interests or personal relationships that could have appeared to influence the work reported in this paper.

Acknowledgment

The authors are grateful to U. Köster for the useful communication.

Appendix A. Supplementary data

Supplementary material related to this article can be found online at https://doi.org/10.1016/j.nima.2020.164989.

References

[1] Neutrons for Science and Technology, Technical Report, European Neutron Scattering Association, 2017.
[2] ESFRI Physical Sciences and Engineering Strategy Working Group, Neutron LandScape Group, ESFRI Scripta I, 2016.
[3] U. Rücker, et al., The Jülich high-brilliance neutron source project, Eur. Phys. J. Plus 131 (2016) 19, http://dx.doi.org/10.1140/epjp/i2016-16019-5.
[4] P. Zakalek, et al., High-brilliance neutron source project, J. Phys.: Conf. Ser. 1401 (2020) 012010, http://dx.doi.org/10.1088/1742-6596/1401/1/012010.
[5] A.J. Koning, D. Rochman, Nucl. Data Sheets 113 (2012) 2841–2934, http://dx.doi.org/10.1016/j.nds.2012.11.002.
[6] P. Zakalek, et al., EPJ Web Conf. 231 (2020) 03006, http://dx.doi.org/10.1051/epjconf/202023103006.
[7] H.J. Brede, et al., Neutron yields from thick be targets bombarded with deuterons or protons, Nucl. Instrum. Methods Phys. Res. A 274 (1989) 332–344, http://dx.doi.org/10.1016/0168-9002(89)90399-9.
[8] M.A. Lone, et al., Thick target neutron yields and spectral distributions from the ^{7}Li(d(p), n) and ^{9}Be(d(p), n) reactions, Nucl. Instrum. Methods Phys. Res. A 143 (1977) 331–344, http://dx.doi.org/10.1016/0029-554X(77)90616-4.
[9] I. Tilquin, et al., Experimental measurements of neutron fluxes produced by proton beams (23–80 MeV) on Be and Pb targets, Nucl. Instrum. Methods Phys. Res. A 545 (2005) 339–343, http://dx.doi.org/10.1016/j.nima.2005.01.325.
[10] Tai, et al., Neutron yields from thick targets bombarded by 18- and 32-Mev protons, Phys. Rev. 109 (1958) 2086, http://dx.doi.org/10.1103/PhysRev.109.2086.
[11] T. Goorley, et al., Initial MCNP6 release overview, Nucl. Technol. 180 (2012) 298–315, http://dx.doi.org/10.13182/NT11-135.
[12] M.B. Chadwick, et al., ENDF/B-VII.1: Nuclear data for science and technology: Cross sections, covariances, fission product yields and decay data, Nucl. Data Sheets 112 (2011) 2887, http://dx.doi.org/10.1016/j.nds.2011.11.002.
[13] R. Maier, Cooler synchrotron COSY – performance and perspectives, Nucl. Instrum. Methods Phys. Res. A 390 (1997) 1–8, http://dx.doi.org/10.1016/S0168-9002(97)00324-0.
[14] W. Bräutigam, et al., H- operation of the cyclotron JULIC as injector for the cooler synchrotron COSY-Jülich, in: Proc. 15th International Conference Cyclotrons'98, Caen, France, 1998, pp. 14–19.
[15] W. Bräutigam, et al., Extraction of D- beams from the cyclotron JULIC for injection into the cooler synchrotron COSY, AIP 600 (2001) 123, http://dx.doi.org/10.1063/1.1435214.
[16] O. Felden, et al., Recent extensions of JULIC for HBS investigations, in: Proc. Cyclotrons'19, 2019, pp. 196–199, http://dx.doi.org/10.18429/JACoW-Cyclotrons2019-TUP019.
[17] Yu. Valdau, et al., IBIC2016 Conference proceedings, 2017, pp. 434–437.
[18] Dr. Westmeier GmbH, HPGe Software, 2020, available at http://www.westmeier.com/hpge-spektrometrie/hpge-software/. (Accessed 11 November 2020).
[19] A. Boston, Introduction to MCNP - the Monte Carlo Transport Code, Version 1.4, University of Liverpool, 2014.
[20] V.T. Astrelin, et al., Blistering of the selected materials irradiated by intense 200 keV proton beam, J. Nucl. Mater. 396 (2010) 43, http://dx.doi.org/10.1016/j.jnucmat.2009.10.051.
[21] Frédéric. Ott, et al., EPJ Web Conf. 231 (2020) 01004, http://dx.doi.org/10.1051/epjconf/202023101004.